# A comprehensive experimental and kinetic modeling study of di-isobutylene isomers: Part 1

Nitin Lokachari, Goutham Kukkadapu, Hwasup Song, Guillaume Vanhove, Maxence Lailliau, Guillaume Dayma, Zeynep Serinyel, Kuiwen Zhang, Roland Dauphin, Brian Etz, et al.

# A comprehensive experimental and kinetic modeling study of di-isobutylene isomers: Part 1

Nitin Lokachari[1,*], Goutham Kukkadapu[2,*], Hwasup Song[3], Guillaume Vanhove[3], Guillaume Dayma[4], Zeynep Serinyel[4], Kuiwen Zhang[2], Roland Dauphin[5], Brian Etz[6], Seonah Kim[7], Mathias Steglich[8], Andras Bodi[8], Gina Fioroni[6], Patrick Hemberger[8], Sergey S. Matveev[9], Alexander A. Konnov[10], Philippe Dagaut[4], Scott W Wagnon[2], William J. Pitz[2], Henry J. Curran[1]

[1] Combustion Chemistry Centre, School of Chemistry, Ryan Institute, MaREI, National University of Ireland Galway, Ireland

[2] Lawrence Livermore National Laboratory, Livermore, CA 94551, USA

[3] Univ. Lille, CNRS, UMR 8522 - PC2A - Physicochimie des Processus de Combustion et de l'Atmosphère, Lille F-59000, France

[4] CNRS-INSIS, Institut de Combustion, Aérothermique, Réactivité et Environnement, Orléans, France

[5] TOTAL Marketing Services, Centre de Recherche de Solaize, Chemin du Canal – BP 22, Solaize 69360, France

[6] National Renewable Energy Laboratory, Golden, CO 80401, USA

[7] National Renewable Energy Laboratory, Golden, CO 80401, and Department of Chemistry, Colorado State University, Fort Collins, CO 80523, USA

[8] Laboratory for Femtochemistry and Synchrotron Radiation, Paul Scherrer Institute, Villigen 5232, Switzerland

[9] Scientific and Educational Centre of Fluid Dynamics Research, Samara National Research University, Samara, Russia

[10] Division of Combustion Physics, Lund University, Lund, Sweden

*Corresponding authors: n.lokachari1@nuigalway.ie, kukkadapu1@llnl.gov

**Abstract**

Di-isobutylene has received significant attention as a promising fuel blendstock, synthesized via biological routes, and is a short-listed molecule for the Co-Optima initiative. Di-isobutylene is also popularly used as an alkene representative in multi-component surrogate models for engine studies of gasoline fuels. However, there is limited experimental data available in the literature for neat di-isobutylene under engine-like conditions. Hence, most existing di-isobutylene models have not been extensively validated, particularly at lower temperatures (< 1000 K). Most gasoline surrogate models include the di-isobutylene sub-mechanism published by Metcalfe et al. [1] with little or no modification. The current study is undertaken to develop a detailed kinetic model for di-isobutylene and validate the model using a wide range of relevant experimental data. Part 1 of this study exclusively focuses on the low- to intermediate temperature kinetics of di-isobutylene. An upcoming part 2 discusses the high-temperature model development and validation of the relevant experimental targets. Ignition delay time measurements for di-isobutylene isomers were performed at pressures ranging from 15 – 30 bar at equivalence ratios of 0.5, 1.0, and 2.0 diluted in air and the temperature range 650 – 900 K using two independent rapid compression machine facilities. In addition, speciation experiments of these isomers were performed in a jet-stirred reactor and in a rapid compression machine. A detailed kinetic model for di-isobutylene isomers is developed to capture the wide range of new experimental targets. For the first time, a comprehensive low-temperature chemistry submodel has been included. The differences in the important reaction pathways for the accurate prediction of the oxidation of the two DIB isomers are compared using reaction path analysis. The most sensitive reactions controlling the ignition delay time of DIB isomers under pressure and temperature conditions necessary for autoignition in engines are identified.

**Keywords**: Di-isobutylene, chemical kinetics, rapid compression machine, jet-stirred reactor, kinetic modeling.

## 1. Introduction

The co-optimization of fuels and engines (Co-Optima) initiative identified fuel properties of blendstocks that can increase the engine efficiency of boosted, spark-ignition (SI) engines when added to a petroleum based fuel [2]. Boosted SI engines operate at higher in-cylinder pressures. Therefore, they require fuels with higher research octane number (RON), octane sensitivity (S), and heat of vaporization (HOV) to avoid undesirable engine knock [3]. A comprehensive evaluation of more than 400 blendstocks from a variety of chemical families, which can also be sourced from biomass [4], followed by a rigorous screening, led to the identification of six blendstocks with fuel properties that, when used in boosted SI engines, can reduce environmental impacts and offer better engine efficiency. Six short-listed fuel blendstocks, with the fewest significant practical barriers for scale-up and commercialization, have been identified: di-isobutylene (DIB), ethanol, iso-butanol, *n*-propanol, *iso*-propanol, and a fusel alcohol blend. This study focuses on investigating the auto-ignition characteristics of DIB.

DIB is a branched alkene (contains one C=C) with an alkyl substitution on the double bond (see Fig. 1) and is often referred to as a mixture of its two isomers 2,4,4-trimethyl-1-pentene (DIB-1) and 2,4,4-trimethyl-2-pentene (DIB-2). DIB has attractive fuel properties for boosted SI engines, such as high RON and octane sensitivity [3]. DIB can be prepared through the dimerization of isobutene, which can be synthesized from bio-derived alcohols, ethanol, or *iso*-butanol [3]. In addition, the DIB isomers received significant attention as simple representatives of alkene compounds in multicomponent surrogate fuels [1, 5-13], which are often formulated to contain one or more representative components from various classes of compounds, including alkanes, alkenes, aromatics, etc., to represent a complex commercial fuel and to simulate real fuels in multidimensional simulations of combustion in engines.

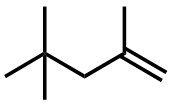

2,4,4-trimethyl-1-pentene
(DIB-1)

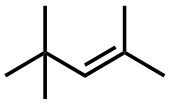

2,4,4-trimethyl-2-pentene
(DIB-2)

**Figure 1**: A two-dimensional representation of DIB isomers.

In addition to their use in surrogate fuels studying the DIB isomers offers kinetic insights into the effect of the presence of an unsaturated bond in *iso*-octane. Alkenes are key intermediates formed during the oxidation of heavier saturated hydrocarbons and constitute a significant portion of commercial transportation fuels. Short-chained alkenes are known to have much higher knock resistance than their alkane counterparts [14]. However, in contrast to alkanes, the combustion kinetics of alkenes are less well studied and understood.

Moreover, most gasoline surrogate models include the DIB-1 sub-mechanism published by Metcalfe et al. [1] which was only validated for temperatures above 1200 K and did not include key reaction pathways relevant to low-temperature combustion. Also, the experimental ignition delay times (IDT) for neat DIB-1 are limited to low pressures and high temperatures. Metcalfe et al. [1] reported IDT experiments at low fuel concentrations (0.375% and 0.75%) in the temperature range 1200 – 1500 K and pressures of 1 – 4 atm. Hu et al. [8] conducted IDT experiments for neat DIB-1 at fuel concentrations ranging from 0.5 – 1.0%, at temperatures in the range 1110 – 1500 K, and pressures in the range of 2 – 10 atm. For experiments where DIB-1 is included as a surrogate component in a mixture, Mittal and Sung [15] performed IDT experiments in an RCM in the temperature range 750 – 1050 K and at pressures of 35 and 45 atm. More recently, high pressure (15 – 30 atm) and low to intermediate temperature (650 – 1000 K) DIB studies were carried out in a rapid compression machine (RCM) [16, 17]. Due to the limited data at low temperatures and high pressures, most literature multicomponent gasoline surrogate models have not been extensively validated for the DIB isomers at engine-relevant pressures and temperatures.

To motivate the current work, simulated results from the kinetic models in the literature are compared to the new experimental IDT data in Fig. 2. The models proposed by Metcalfe et al. [1] and Li et al. [9] are in relatively good agreement with the new experimental data in the temperature range 900 – 1350 K, while poor quantitative predictions are observed for several multi-component surrogate models. Due to the lack of comprehensive low-temperature oxidation (LTO) chemistry and lack of knowledge about the DIB allylic radical decompositions, most of the multicomponent surrogate models considered for this study could not reproduce the new experimental data over the whole investigated temperature range in Fig. 2. Recently, Lokachari et al. [18] highlighted the significant hierarchical dependence of the DIB-1 oxidation mechanism on the underlying isobutene kinetics, which is a critical intermediate formed in the decomposition of DIB-1, particularly at high temperatures (> 1000 K). The influence of isobutene kinetics on the predictions of IDTs and laminar burning velocities (LBV) for DIB-1 oxidation has also been reported recently by Lokachari et al. [18] and it was concluded that isobutene kinetics largely controls the high temperature oxidation of DIB-1.

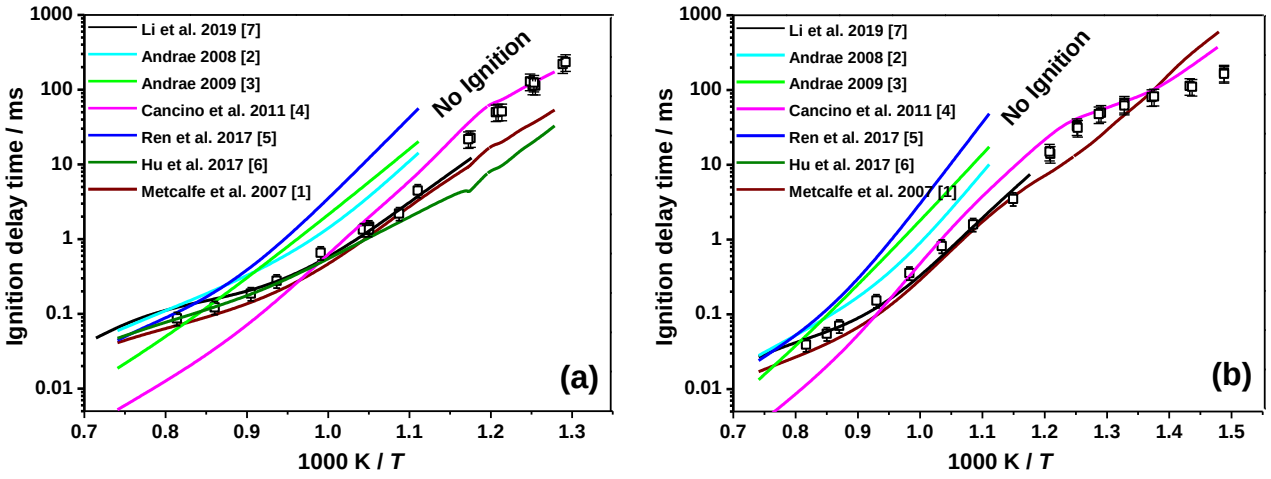


**Figure 2:** Validation of literature multi-component surrogate models against new DIB-1 IDT experiments (open squares) performed in the shock-tube and rapid compression machine at NUIG for fuel in air mixtures at $\varphi$ = 1.0 and (a) $p$c = 15 and (b) $p$c = 30 bar.

The development of a comprehensive chemical kinetic mechanism for the DIB isomers and its validation using a wide range of reliable experimental targets is the main objective of the current study. This paper (part 1) exclusively focuses on the model development and validation of low to intermediate temperature experimental data of the DIB isomers, using IDT measurements performed in two independent laboratories and speciation data from a jet-stirred reactor (JSR) and RCM are also included in this paper. The upcoming part-2 [19] (in preparation) focusses on the high temperature oxidation chemistry of the DIB isomers using relevant experimental validation datasets from various other fundamental reactors.

## 2. Experimental methods

To understand the oxidation chemistry and the ignition propensity of DIB, speciation and ignition delay measurements (IDT) were conducted in RCM's and JSR. The IDT measurements were acquired using two separate RCM facilities at NUI Galway and ULille. Speciation experiments were performed in an RCM at ULille and a JSR at ICARE Orléans. The details of the conditions of the experiments performed are listed in Tables 1 – 3.

### 2.1. Rapid Compression Machine (NUIG)

The RCM at NUIG is employed to complement the HPST experiments to measure IDTs in the low to intermediate temperature regime (650 – 900 K), with the experimental details provided in Table 1. The test fuel (DIB-1 98.5%) was supplied by Sigma Aldrich®. The other gases used in this study, nitrogen (99.99%), oxygen (99.99%), argon (99.96%), and helium (99.97%), were purchased from BOC Ireland. Homogeneous fuel-air mixtures were prepared in an external stainless-steel vessel maintained at ~50 °C to prevent fuel condensation and allowing the fuel-air to diffusively mix for at least 12 h before performing the experiments. The RCM has an opposed twin-piston arrangement with 38 mm bore and 168 mm stroke. Briefly, the pre-mixed fuel/air mixture is introduced into the reaction chamber and is rapidly compressed (~16 ms) by the pistons. Creviced piston heads were used to largely limit the turbulence/roll-up vortices generated in the test gas. The pistons are

pneumatically driven and locked at the end of compression, creating a constant volume condition. After compression, the pressure drops due to heat loss from the gas mixture to the reaction chamber walls. Thus, to isolate the heat-transfer effects, pyrolytic (non-reactive) pressure profiles are recorded by replacing $O_2$ with $N_2$ to account for the heat loss effects in the simulations.

A range of compressed gas temperatures is obtained by varying the initial temperature of the RCM system to temperatures not greater than 150 °C, to avoid damaging the seals within the system. To further achieve higher compressed temperatures, a 50% $N_2$/50% Ar diluent ratio was used. IDT and compressed pressure are measured using a Kistler 603CAB sensor mounted on the sidewall of the reaction chamber. The 'adiabatic compression/expansion' routine in Gaseq [20] was used to calculate the compressed temperature. The sample experimental pressure traces for DIB isomers are depicted in Fig. 3. Summary of the NUIG experimental test matrix is shown in Table 1, and more detailed information on the composition, inlet pressure, inlet pressure along with the volume histories are provided in the supplementary material.

**Table 1**: List of experimental conditions and the molar composition of the test fuel/oxidixzer composition studied for DIB-1.

| $\varphi$ | Fuel (%) | $O_2$ (%) | $N_2$ + Ar (%) | Compressed pressure (bar) |
|---|---|---|---|---|
| 0.5 | 0.87 | 20.82 | 78.31 | 15, 30 |
| 1.0 | 1.72 | 20.64 | 77.64 | 15, 20, 25, 30 |
| 2.0 | 3.38 | 20.29 | 76.33 | 15, 30 |

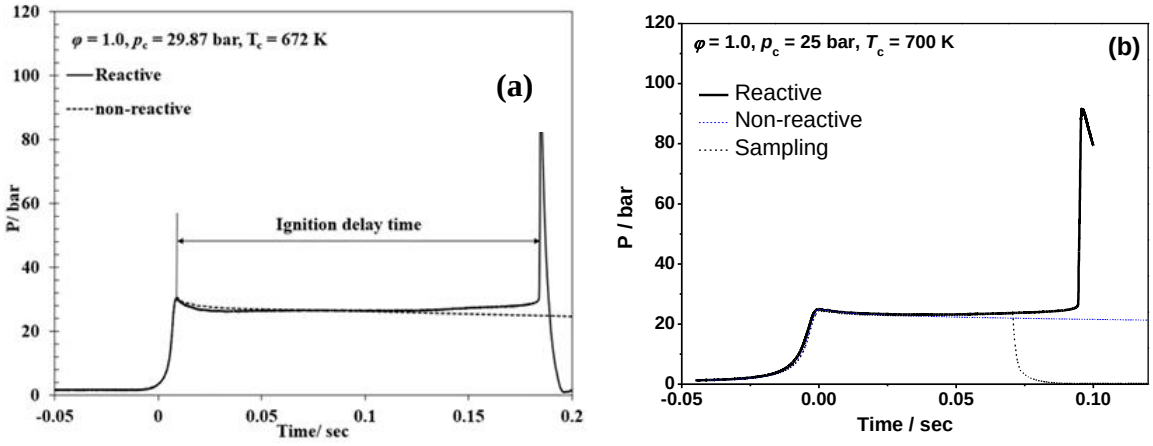


**Figure 3:** Sample RCM pressure traces measured (a) DIB-1 at NUIG and (b) DIB-2 at ULille.

### 2.2. Rapid Compression Machine (ULille)

The ULille RCM has been utilized for decades to measure IDTs of a wide variety of fuels, as well as to perform speciation measurements to track the evolution of the stable species formed during the ignition delay period and provide direct kinetic insights to construct and validate a reaction mechanism, as demonstrated in recent studies [21-23]. The driving piston, which is run by compressed air and stopped by hydraulics, and the driven piston are connected at a right angle on the same plane by a grooved metallic cam. The advantages of this design are that the compression-time history is reproducible with repeated experiments and that the piston rebound at the end of compression is suppressed as the grooved section of the cam holds the driven piston at its top dead centre (TDC) position. In addition, the driven piston is equipped with a creviced piston head [24] to maintain temperature homogeneity after the compression phase by absorbing the thermal boundary layer developed during the compression stroke by suppressing roll-up vortex formation [25, 26]. With a 50 mm bore and 200 mm stroke, the combustion chamber is heated by multiple electric band heating elements. The axial deviation of the in-cylinder temperature is carefully adjusted to remain within 1 K, which leads to a maximum compressed temperature deviation of $2-2.5$ K, depending on the mixture composition. The compression ratio is adjustable by installing different end plates at the top of the combustion chamber to modify the clearance height and was fixed at 10.3 for this work. A thermal shock-protected piezoelectric pressure transducer (Kistler 601CA) was coupled with a charge amplifier (Kistler 5007) to record the pressure-time history during the experiments. For the mixture preparation, high purity DIB isomers, i.e., DIB-1 (> 99%, Acros Organics) and DIB-2 (> 98%, Acros Organics), were treated with repeated freeze-thaw distillation to remove any dissolved gases, and all the gaseous components, i.e., Ar, $N_2$, and $O_2$, were supplied by Air Liquide ($\geq$ 99.99%).

**Table 2**: List of experimental conditions studied at ULille RCM for DIB-1 and DIB-2 IDTs at $\varphi$ = 1.0 and 15, 20 and 25 bar in the range of $T_C$ = 660 – 900 K.

| DIB (%) | $O_2$ (%) | $N_2$ (%) | Ar (%) | $CO_2$ (%) |
|---|---|---|---|---|
| 1.72 | 20.64 | 0.00 | 77.63 | 0.00 |
| 1.72 | 20.64 | 6.99 | 70.64 | 0.00 |
| 1.72 | 20.64 | 13.20 | 64.40 | 0.00 |
| 1.72 | 20.64 | 20.96 | 56.67 | 0.00 |
| 1.72 | 20.64 | 29.50 | 48.13 | 0.00 |
| 1.72 | 20.64 | 38.82 | 38.82 | 0.00 |
| 1.72 | 20.64 | 46.58 | 31.05 | 0.00 |
| 1.72 | 20.64 | 54.34 | 23.30 | 0.00 |
| 1.72 | 20.64 | 62.11 | 15.53 | 0.00 |
| 1.72 | 20.64 | 69.87 | 7.76 | 0.00 |
| 1.72 | 20.64 | 77.63 | 0.00 | 0.00 |
| 1.72 | 20.64 | 71.42 | 0.00 | 6.20 |

In addition, sampling and speciation experiments were conducted to provide detailed experimental evidence for validating the DIB kinetic model by observing the formation of stable intermediates at $T$c = 700 ± 2 K, $p_C$ = 25 ± 0.5 bar, and $\varphi$ =1.0. Comparing the speciation results from the isomers helps to develop their kinetic models, especially when their structure-specific intermediates are expected in large quantities. For example, C=C double bond-specific reaction pathways for alkenes at low-to-intermediate temperatures were experimentally validated in previous studies regarding a mixture of DIB-1 and DIB-2 [17] and the linear hexene isomers [27]. Reacting mixture sampling is realized by a sudden expansion of the compressed volume during the ignition delay period, thereby quenching reactions and freezing the composition thanks to the superior volume ratio of 40 (sampling canister) to 1 (the volume of the fully compressed combustion chamber). Samples were taken near 0.84 (for DIB-1) and 0.70 (for DIB-2) of the normalized time of the total IDT at the condition above for each isomer. Once the sample was taken, it was immediately injected into two gas chromatographs; a primary Bruker Scion 456 equipped with a mass spectrometer (MS), a thermal conductivity detector (TCD), and a flame ionization detector (FID) along with BR-5 and PoraBond-Q columns for the separation of heavy and light hydrocarbons along, and a secondary Agilent 6890 with a molecular sieve and TCD/FID for the detection of permanent

gases and CO. The effective carbon number (ECN) concept was applied to derive the mole fractions of different intermediates from the FID response signal [28], with an uncertainty estimated to be within ± 15%.

Selectivities of the intermediates were calculated by normalizing the mole fraction of the ~~interesting species by the sum of all the~~ identified intermediates. In detail, the following equation is used,

$$s_i = \frac{x_i}{\sum_{i=1}^{N} x_i}$$

$S_i$ denotes the selectivity of the $i^{th}$ species and $x_i$ is the mole fraction of the $i^{th}$ species, respectively. Since the maximum achievable TDC pressure is slightly lower than 25 bar when the sampling apparatus is installed, the relevant IDT at the sampling condition is slightly longer than the corresponding non-sampling condition.

### 2.3. Jet stirred reactor (ICARE-Orléans)

The oxidation of DIB (neat DIB-1 and a mixture of 75% DIB-1 and 25% DIB-2 by mole) was carried out in a fused silica JSR. This setup can be used for studies at pressures going up to 10 atm and temperatures up to 1280 K. The fuel was handled using an HPLC pump, atomized, and vaporized through heated grids in a nitrogen flow and then carried to the reactor by a quartz capillary. The fuel is highly diluted to avoid strong heat release. The oxidizing mixture ($N_2$+$O_2$) is conveyed to the reactor separately to avoid any premature reactivity. The two flows meet at the entrance of the injectors and are mixed by high turbulence generated by four nozzles. Temperature is monitored by a Pt-Pt/Rh-10% thermocouple isolated from the gases by a quartz sheath to avoid any catalytic reaction. A low-pressure sonic probe is used to sample the reactor and freeze the reactivity. The samples are then analyzed online by Fourier transform infrared spectroscopy (FTIR) or stored at low-pressure in 1 L Pyrex bulb for further gas chromatograph (GC) analyses. Off-line analyses were performed using GCs equipped with capillary columns (0.32 mm i.d.: DB-624 and CP-Al2O3-KCl, and 0.53 mm i.d.: Carboplot-P7), a thermal conductivity detector (TCD), and a flame ionization

detector (FID). A GC-MS (Varian quadrupole V1200) operating with electron ionization (70 eV) was used for product identification. More details regarding this setup can be found in the literature [29].

**Table 3**: Experimental conditions investigated in the JSR.

| | | |
|---|---|---|
| Equivalence ratio ($\varphi$) | 0.5, 1.0 and 2.0 | 0.5 and 1.0 |
| Test mixture composition | 1000 ppm neat DIB-1 | 750 ppm DIB-1 + 250 ppm DIB-2 |
| Residence time ($\tau$) | 0.7 sec | 0.7 sec |
| Pressure ($p$) | 10 atm | 10 atm |
| Temperature ($T$) | 700 – 1200 K | 700 – 1200 K |

The mole fraction profiles of the reactants (DIB-1, DIB-2, and $O_2$) and products ($H_2$, $H_2O$, CO, $CO_2$, $CH_2O$, $CH_4$, $C_2H_4$, $C_2H_6$, $C_2H_2$, $C_3H_6$, isobutene, 2-methyl but-1-ene, isoprene, $CH_3CHO$, acrolein, 2-methylpropanal, methacrolein, acetone, methyl vinyl ketone, and benzene) were measured by FTIR and gas chromatography. Uncertainties regarding the results can be attributed to temperature measurements within the reactor (± 5 K), the reactants and diluent flow rates, and the analyses. The total uncertainty in species mole fractions is challenging to quantify but can be estimated to be ± 15%. The elemental balance is checked at the end of each experiment and stays within 10% for carbon, hydrogen, and 15% oxygen.

Experiments were carried out at steady state, 10 atm, at constant residence time $\tau$ = 0.7s, and equivalence ratios of 0.5, 1.0, and 2.0 for pure DIB-1, and 0.5 and 1.0 for the DIB mixture. The initial fuel mole fraction was held constant (1000 ppm), and temperatures ranged from 720 – 1200 K in 30 K increments.

## 3. Kinetic Modeling

The chemistry of alkenes at low and intermediate temperatures is more complicated than alkanes due to the C=C double bond, as H-atom abstraction forms allylic and vinylic radicals and the addition of radicals to the double bond becomes possible. The rate constants of many of these $C_8$ allylic radical decompositions are not well known. Moreover, the low-temperature mechanism describing alkene combustion contains hundreds of species and thousands of elementary reactions, each of

which are assigned thermodynamic properties and rate constant expressions, respectively. Unfortunately, there is very little or no experimental data on most of these properties. Thus, kineticists rely primarily on theoretical studies to provide the rate constant and thermodynamic property data for the oxidation of alkenes, and to develop rate rules for various reaction classes necessary to describe alkene low-temperature combustion.

The DIB models have been developed as a collaborative effort between NUIG and LLNL. The small hydrocarbon ($C_0 - C_4$) base chemistry has been adapted from the recent study by Lokachari et al. [18], while the $C_5$ and $C_6$ species chemistry is adopted from Bugler et al. [30] and Zhang et al. [31], respectively. Since the DIB isomers are intermediates formed during the oxidation of iso-octane, the recent iso-octane sub-mechanism is adopted from Fang et al. [32]. The high temperature chemistry of DIB-1 is majorly dependent on an accurate kinetic description of isobutene chemistry, whose kinetic parameters have been re-assessed [18] by incorporating the rates and thermochemical properties from recent advances from ab-initio studies and experimental diagnostics. The description of the kinetic model development below will mainly focus on the key reaction classes. An additional description focusing on the high temperature part of the DIB mechanism is given in Part 2 [19]. In this study, the thermochemical data has been calculated for all of the species of interest to DIB oxidation using Benson's group additivity method using the THERM software [33] based on the group values from the recent publications [34, 35].

### 3.1. H-atom abstraction reactions

H-atom abstraction reactions from the DIB isomers are dominated by abstractions from the allylic sites due to the combination of the relatively weaker allylic C–H bonds and their high degeneracy. DIB-1 has five allylic hydrogen atoms and nine primary hydrogen atoms, whereas DIB-2 has six allylic hydrogen atoms and nine primary hydrogen atoms. H-atom abstractions from an allylic carbon atom are the most facile at low temperatures due to their relatively low C–H bond energy. Abstraction from alkyl sites are the next important abstraction reactions followed by the abstraction

of vinylic hydrogen atoms. The analogous propene/isobutene rate parameters were used for primary allylic H-atom abstraction by Ö, ȮH and HȮ$_2$ radicals, and $O_2$ from various studies [18, 36-38]. To simulate H-atom abstraction reactions from the secondary allylic site, respective 1-butene ($C_4H_8$-1) analogies were used [37, 39, 40]. The rate constants for abstraction of the primary hydrogens were adapted by analogy with iso-octane kinetics [41, 42], assuming that the presence of the C=C double bond has no influence, given its distance from these atoms. The abstractions from the vinylic sites have been modelled using analogies with the $C_1$–$C_4$ core mechanism.

### 3.2. Intra-molecular H-atom shifts of DIB radicals

Allylic and alkylic DIB radicals formed from H-atom abstraction reactions can interconvert through intramolecular H-atom shift reactions, which occur during alkene pyrolysis and oxidation. In the current model, high-pressure rate constants of intramolecular H-atom shift reactions of both alkyl and allylic radicals were adapted from a recent theoretical investigation by Wang et al. [43] using electronic structure calculations at the CBS-QB3 level of theory.

### 3.3. Radical addition to molecular oxygen

The addition of allylic fuel radicals to $O_2$ is less facile than for their non-allylic radical [44-46] counterparts. However, the chemistry subsequent to allylic radical addition to $O_2$ has been shown to be important in accurately predicting the ignition propensity of isobutene [18]. For this reason, the addition of allylic DIB radicals to $O_2$ molecules leading to the formation of alkenyl-peroxy radicals are included in the mechanism, and have been modelled by analogy with isobutene from Chen and Bozzelli [47]. The following reactions, which include intramolecular H-atom shift reactions to form hydro-peroxy alkyl radicals (ȮOOH) and the second radical addition reactions to $O_2$ are adapted from Chen and Bozzelli. Non-allylic radicals, that can readily add to $O_2$ at low temperatures forming alkyl-peroxy ($iC_8D_4$-1Ȯ$_2$R, $iC_8D_3$-1Ȯ$_2$R) radicals, can eventually produce carbonyl-hydroperoxides and ȮH radicals through a series of internal H-atom isomerization and radical addition to $O_2$ reactions. This combined low temperature reaction sequence is expected to contribute to the low

temperature reactivity of the DIB isomers, and the relevant reaction rate coefficients were derived from reaction rate rules developed for alkanes [48].

### 3.4. Cyclo-addition reactions of alkenyl-peroxy radicals

The present mechanism describes the formation of cyclo-peroxy alkyl radicals produced from intramolecular cyclo-addition reactions of the peroxy group onto the double bond. This class of reactions which was rarely modelled in earlier literature mechanisms was found to be important in the recent kinetic modelling of isobutene and linear pentene isomers. Therefore, for completeness in the model, these reactions are included using the rate constants from a recent high-level calculation from Sun et al. [49].

### 3.5. Reactions of allylic and $H\dot{O}_2$ radicals

Previous studies [44, 50, 51] have concluded that allylic radicals react with $H\dot{O}_2$ radicals and decompose or undergo chemically activated channels to produce alkenoxy and hydroxyl radicals. These reactions convert less reactive $H\dot{O}_2$ radicals into reactive $\dot{O}H$ radicals, promoting reactivity at low and intermediate temperatures. The kinetic model developed in this work has adopted the pathway of recombination followed by decomposition to allyloxy radical + $\dot{O}H$, and the chemically activated pathway, with the reaction rates taken by analogy with propene oxidation kinetics [50].

### 3.6. Radical addition to the double bond

#### 3.6.1. $\dot{O}H$ radical addition

In the low-to-intermediate temperature regime, the presence of the C=C double bond can enable an $\dot{O}H$ radical addition pathway, producing alcoholic radicals that can then add to $O_2$ to form hydroxy alkyl-peroxy (HAP) radicals. The HAP radical so formed can proceed through the Waddington mechanism, which involves an internal H-atom transfer from the hydroxyl site, followed by decomposition into two aldehyde molecules and one $\dot{O}H$ radical. However, the hydrogen atom may also be transferred from a carbon atom rather than from the $\dot{O}H$ group, which is similar to a typical

$R\dot{O}_2$ isomerization reaction in the low temperature oxidation of alkanes. In this way, the addition of ȮH radicals to the double bond in an alkene can initiate alkane-like low temperature reaction pathways [48]. In assigning the associated rate constants to these pathyways, ȮH addition to the C=C double bond was taken by analogy to ȮH addition to propene from [52] with a branching ratio of 75:25, favoring addition to the terminal carbon atom. Rate constant expressions for the next steps of radical additions to $O_2$, internal isomerization, dissociation reactions, and alternate Waddington pathways were modeled using analogous rate constants to those by Sun et al. [53].

### 3.6.2. $H\dot{O}_2$ radical addition

$H\dot{O}_2$ radical concentrations are relatively high at intermediate temperatures (750 – 1000 K) [37], and these can recombine with allylic radicals or add on to the double bond forming hydroperoxy alkyl radicals. To describe $H\dot{O}_2$ radical additions to the double bond, analogous to ethylene and isobutene rate constants were taken from the calculations by Zádor et al. [37] for internal and terminal additions, respectively.

### 3.6.3. Ḣ atom addition

H-atom addition to the C=C double bond in the DIB isomers forming iso-octane radicals was modeled as the decomposition of iso-octane radicals adopting the analogous rate constants from Wang et al. [54].

## 4. Results and discussion

The IDTs for DIB isomers were measured in both RCMs at pressures and temperatures relevant to practical applications, i.e., 15 – 30 bar and 650 – 900 K at equivalence ratios in the range of 0.5 – 2.0. The IDT data exhibited no negative temperature coefficient (NTC) behavior in the temperature range investigated, and the logarithm of IDT varies non-linearly with the inverse temperature, Figs. 4(a) – 4(d). The model can well reproduce the IDT experiments from two independent RCM facilities; Fig. 4(b) represents common experiments (for DIB-1) and simulations using the corresponding heat loss

profiles. In Fig. 4(b), the solid and open symbols represent the IDT experiments using ULille RCM and NUIG RCM respectively. Simulations were performed including the corresponding heat loss profiles i.e., solid and dashed lines represent ULille and NUIG data, respectively, however, the model is slightly faster (~25%) than the experiments in the temperature range of 715 – 770 K for all pressures.

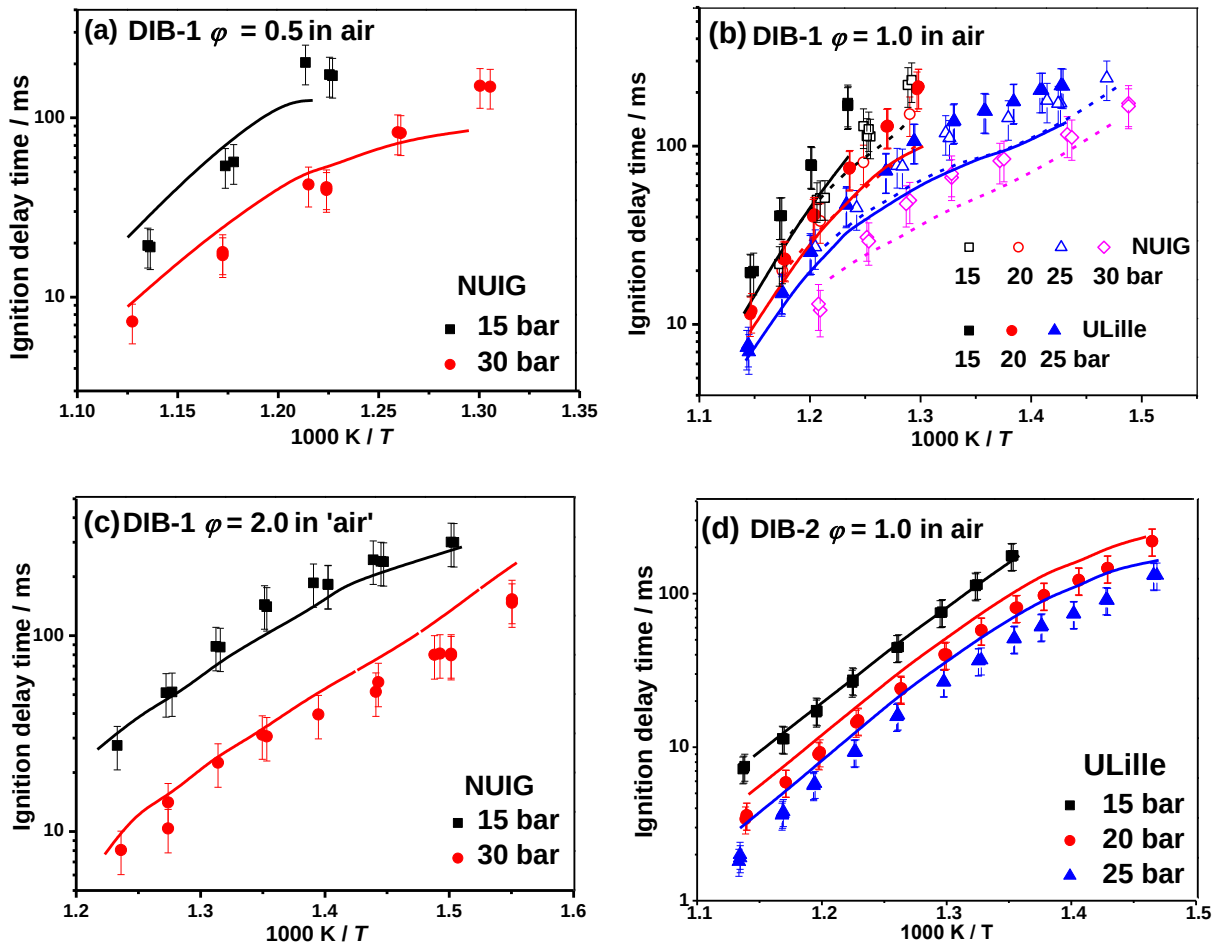


**Figure 4:** The current model predictions for DIB isomers; IDTs measured at NUIG and ULille RCM at (a) DIB-1 $\varphi$ = 0.5, (b) DIB-1 $\varphi$ = 1.0, (c) DIB-1 $\varphi$ = 2.0 and (d) DIB-2 $\varphi$ = 1.0 at pressures ranging from 15 – 30 bar.

### 4.1. DIB-1 kinetic analyses

Figure 5 depicts the main reaction pathways of DIB-1 (**1**) at $\varphi$ = 1.0, 800 K, 30 bar condition at the time of 20% fuel conversion. In total, 73% of DIB-1 undergoes H-atom abstraction reactions, of which 35%, 22%, and 16% of the fuel abstraction form secondary allylic (**2**), alkyl (**3**), and primary

allylic (**4**) radicals, respectively. Radical addition reactions to the C=C double bond corresponds to approximately 26%, of which 17% comes from ȮH radicals (**5,6**), with 9% coming from Ḣ atoms, (7). Most of the flux (~80%) of the secondary allylic radical of DIB-1 ($iC_8D_3$-5R) proceeds via β-scission, forming a $C_7$ diene (**9**) and methyl radicals. Other minor channels (~6%) include $HȮ_2$ radical addition to the allylic site followed by dissociation to form allyloxy and ȮH radicals. Interestingly, 45% of the primary allylic radicals formed from DIB-1 ($iC_8D_4$-5R, **4**) undergo an intra-molecular H-atom shift to form alkyl radicals ($iC_8D_4$-1R, **3**). The DIB-1 alkyl radicals (**3**) can undergo β-scission (~53%) to form isobutene and 2-methyl allyl radicals (**10**) or addition to $O_2$ (46%) to form alkenyl peroxy radicals (**11**). These alkenyl peroxy radicals undergo typical low temperature kinetics at these temperature and pressure conditions, including internal isomerization, second $O_2$ addition, and further isomerization, leading to low-temperature chain branching.

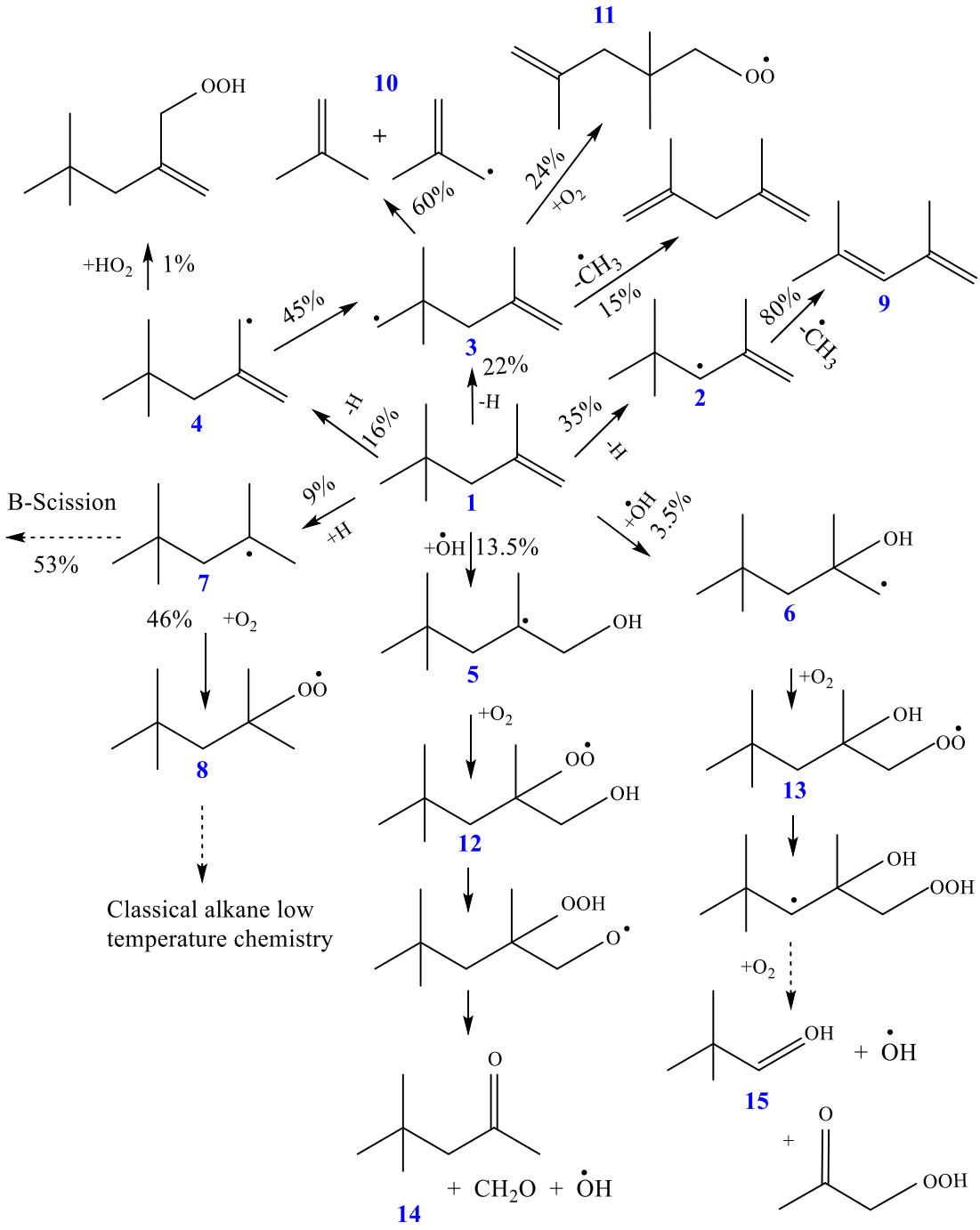


**Figure 5:** Flux analysis using the current model for DIB-1 oxidation at $\varphi$ = 1.0 in air, 30 bar at 800 K at the time of 20% fuel consumption.

Generally, addition reactions have smaller activation energies compared to abstraction reactions, and hence addition reactions tend to dominate at low to intermediate temperatures, with abstraction reactions dominating at high temperatures. Approximately 9% of DIB-1 forms a tertiary iso-octyl

radical ($iC_8$-4R, **7**) via Ḣ atom addition to the terminal C=C bond. 53% of $iC_8$-4R dissociates via β-scission forming $iC_4H_8$ and $t\dot{C}_4H_9$ radicals (not shown in Fig. 5), and 46% of flux forms iso-octyl peroxy radicals (**8**), which follow typical alkane low temperature oxidation, which is part of the iso-octane sub-mechanism. Terminal and internal ȮH radical addition to the C=C bond accounts for 13.5% and 3.5% respectively, of DIB-1 flux, and the hydroxy alkyl radicals (**5, 6**) formed further react with $O_2$. Thus formed hydroxy alkyl peroxy radicals (**12**) follow the Waddington mechanism via an internal H-atom shift from the ȮH site to the peroxy site followed by the prompt dissociation of the alkoxy radical to two carbonyl species and ȮH radicals (**14**). However, an alternate pathway involving an intra-molecular H-atom shift forming a 6-membered transition state (TS) can compete with the Waddington mechanism. As seen in Fig. 5, for the DIB-1 hydroxy alkyl peroxy species with internal ȮH addition and terminal $O_2$ addition ($iC_8OH4\text{-}5O_2R$, **13**), alternative pathways are found to be dominant as they involve an H-atom shift from a secondary carbon site, and because 6-membered TS have a smaller energy barrier compared to an H-atom shift from the hydroxyl radical. The radicals produced react with $O_2$, ultimately dissociate to form hydro-peroxy acetone ($C_3$KET21), 2,2 di-methyl propanal ($tC_4H_9CHO$), and ȮH radicals (**15**) and thus contribute to the low temperature reactivity of DIB-1.

Figure 6 presents the most sensitive reactions controlling IDTs at 800 K, the self-recombination of $H\dot{O}_2$ radicals inhibits reactivity at these conditions, as it consumes two radicals to form two stable ($H_2O_2$ and $O_2$) molecules. Also, the β-scission reactions of DIB-1 radicals ($iC_8D_4$-1R) inhibit reactivity, as they compete with $O_2$ addition pathways which contribute to greater reactivity at low temperatures. Methyl radicals, mainly produced from the β-scission of DIB-1 radicals ($iC_8$D4-1R and $iC_8$D3-5R), accumulate and react with $O_2$ forming methyl peroxy ($CH_3\dot{O}_2$) radicals. H-atom abstraction by $CH_3\dot{O}_2$ and $H\dot{O}_2$ radicals tend to increase reactivity at these conditions. This is due to the dissociation of $CH_3O_2H$ and $H_2O_2$ to $CH_3\dot{O}$ + ȮH and ȮH + ȮH, producing reactive radicals.

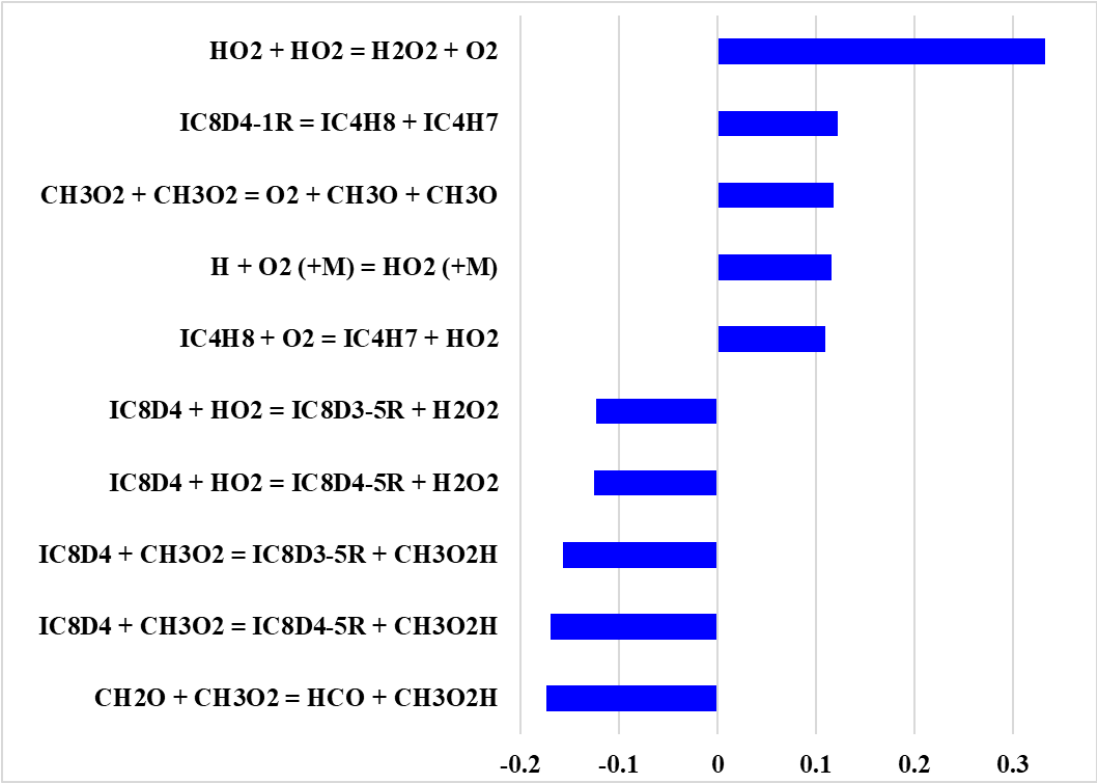


**Figure 6**: Brute force sensitivity analysis representing reactions controlling DIB-1 IDTs using the new model at $\varphi$ = 1.0 in air, *pc* = 30 bar, and *Tc* = 800 K.

### 4.2. DIB-2 kinetic analyses

The flux analysis using the current model for DIB-2 oxidation at $\varphi$ = 1.0, 30 bar and 800 K, at 20% fuel consumption is depicted in Fig. 7. The DIB-2 isomer (**1**) is mainly consumed via H-abstraction reactions at the primary allylic (37%) and alkylic (24%) sites, forming radicals **2** and **3** respectively. The rest of the DIB-2 flux is consumed via addition reactions, 8% via H-addition at the secondary vinylic position with the double methyl substitution, forming $iC_8$-4R (**4**). $iC_8$-4R undergoes β-scission (56%), producing $iC_4H_8$ and $t\dot{C}_4H_9$, while the remaining 44% undergoes $O_2$ addition (**5**) and classical low temperature chain branching kinetics. ȮH radical addition reactions to the C=C bond account for 13.5% and 4.5% of DIB-2 flux, forming hydroxy alkyl radicals (**6)** and **(7)** respectively. These hydroxy alkyl radicals react with $O_2$ and undergo the Waddington mechanism producing acetone 2,2-dimethyl propanal ($tC_4H_9CHO$) and ȮH, (**8**). About 72% of the allylic radical of DIB-2 ($iC_8D_3$-5R) proceeds via β-scission, forming a $C_7$ diene and methyl radical, (**9**).

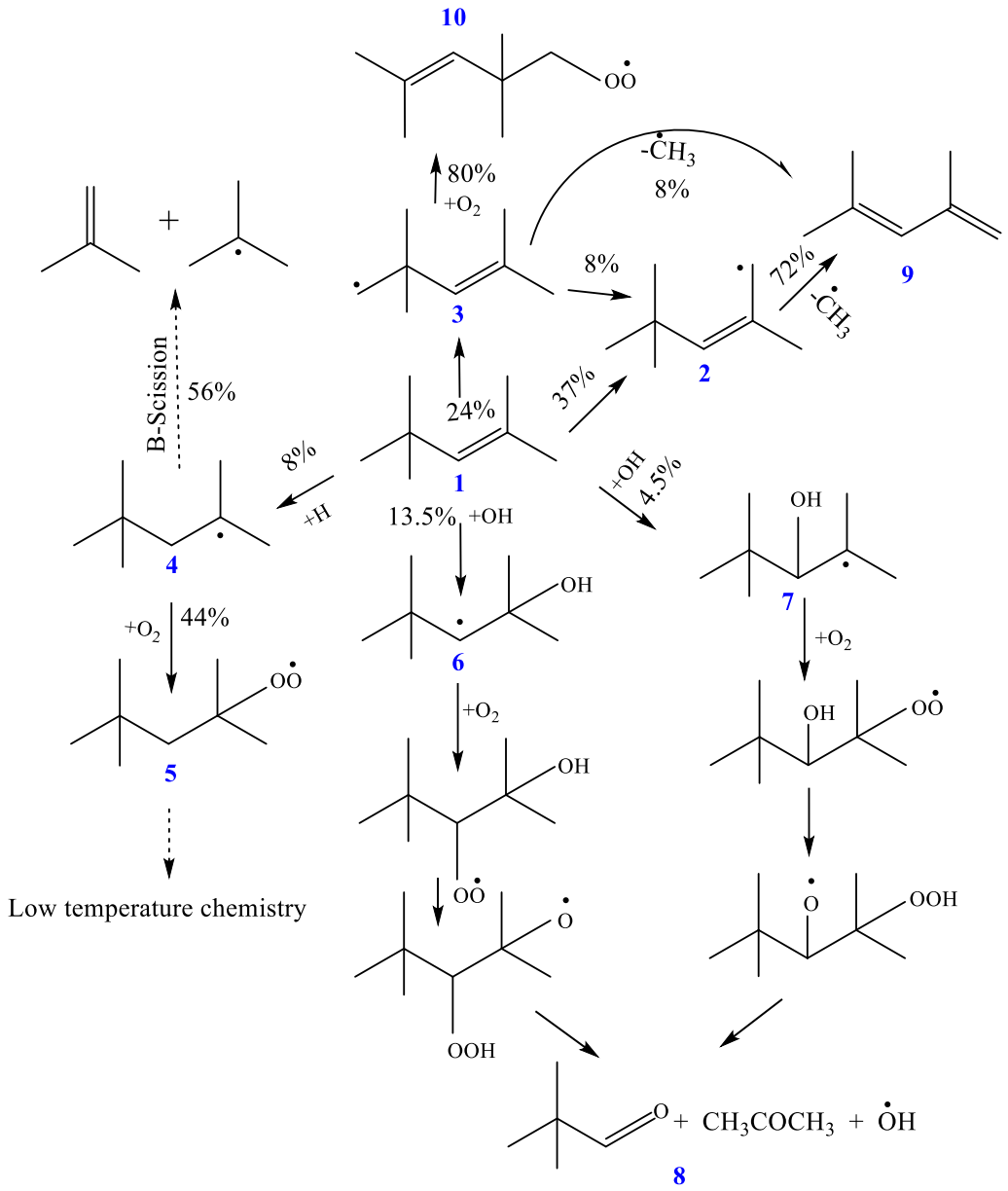


**Figure 7**: Flux analysis using the current model for DIB-2 oxidation at $\varphi$ = 1.0 in air, 30 bar at 800 K, and 20% fuel consumption.

Figure 8 presents the sensitive reactions controlling DIB-2 IDTs at $\varphi$ = 1.0, 30 bar, and 800 K. Similar to DIB-1, the self-recombination reactions of $H\dot{O}_2$ and $CH_3\dot{O}_2$ radicals inhibit reactivity. In contrast, H-atom abstraction by $CH_3\dot{O}_2$ promotes reactivity at these conditions. The other promoting reactions include $\dot{O}H$ addition to the DIB-2 producing $iC_8OH4\text{-}3R$, and several $\dot{O}H$ addition pathways are potentially viable. After subsequent $O_2$ addition at the secondary carbon, the resulting $R\dot{O}_2$ species can undergo several six-membered ring H-shifts, one of which includes the Waddington

mechanism involving the H-shift from the hydroxyl group leading to the formation of $tC_4H_9CHO$, $CH_3COCH_3$, and ȮH. A six-membered ring H-shift is also possible from the double methyl substituted groups, followed by a second $O_2$ addition and isomerization to ultimately produce two ȮH radicals, thus enhancing the reactivity at these conditions.

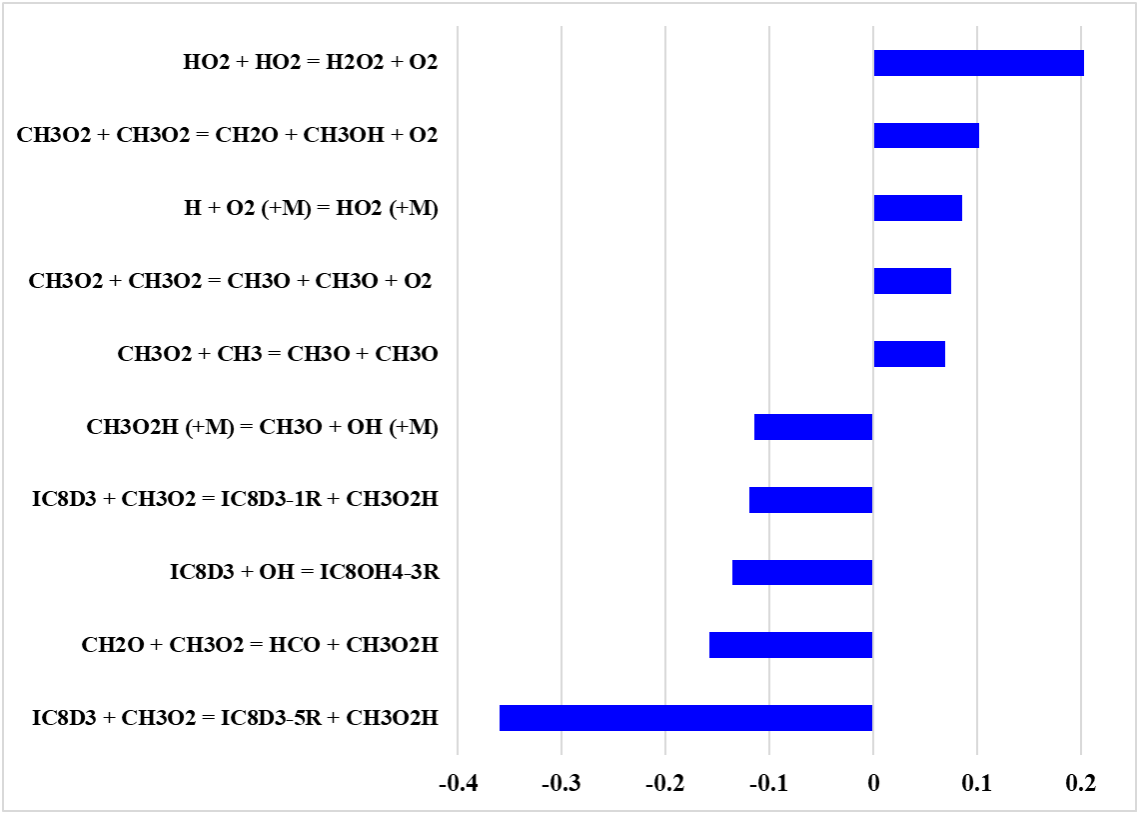


**Figure 8**: Brute force sensitivity analysis representing reactions controlling DIB-2 IDTs using the new model at $\varphi$ = 1.0 in air, $p_C$ = 30 bar, and $T_C$ = 800 K.

### 4.3. Reactivity comparison of DIB isomers

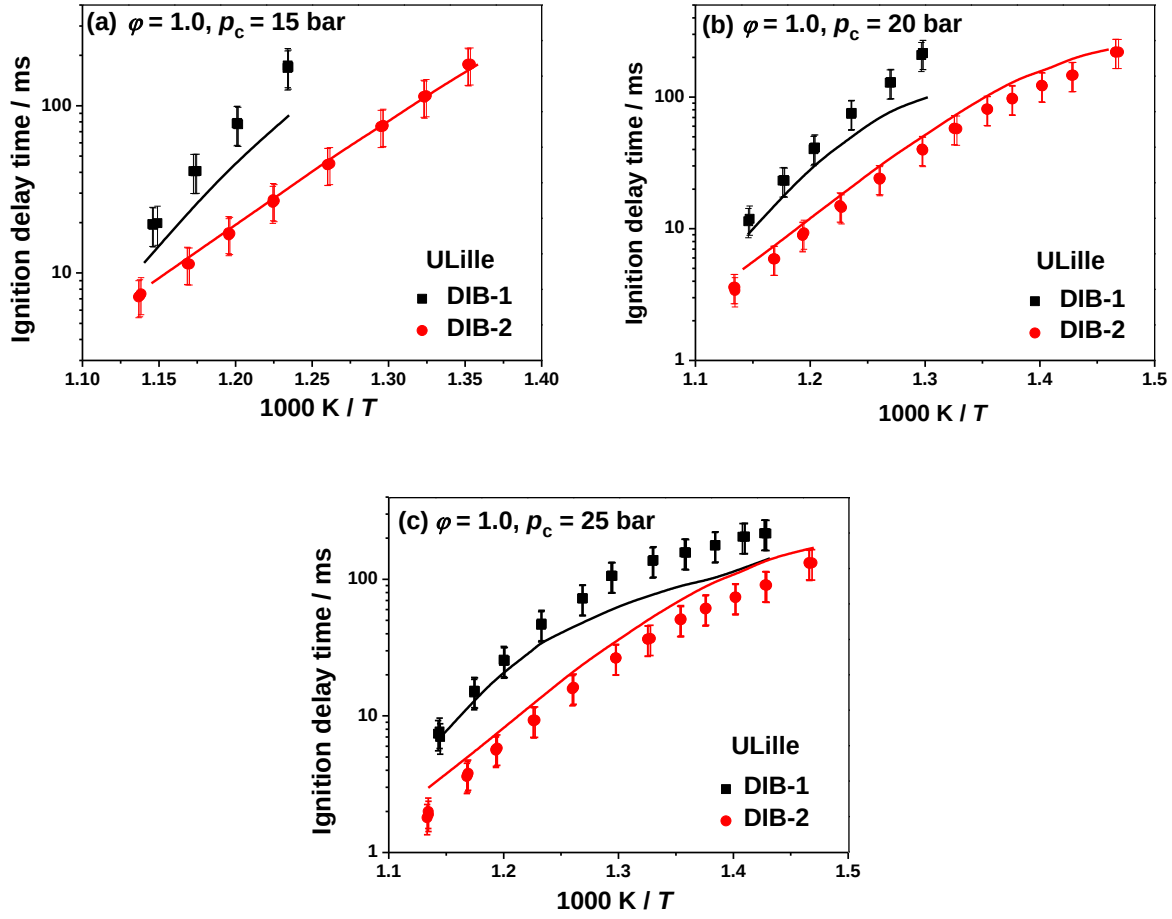


**Figure 9:** The current model predictions for DIB isomers; IDTs measured at ULille RCM at $\varphi$ = 1.0 fuel in air at (a) 15, (b) 20 and (c) 25 bar.

Reactivity comparisons using the experimental IDTs (ULille) of stoichiometric ($\varphi$ = 1.0) DIB-1 and DIB-2 in air mixtures at 15, 20, and 25 bar are presented in Figs. 9(a) – 9(c). In the investigated $p_C/T_C$ conditions, DIB-2 exhibited faster reactivity (lower IDTs) than DIB-1. The position of the double bond in the DIB isomers, therefore, influences the reactivity. The relatively low C–H bond dissociation energy (BDE) at the allylic sites for DIB isomers favour the H-abstraction reactions, as the products formed are resonantly stabilized. DIB-2 has more abstactable sites (6-primary allylic + 9 primary alkylic) than DIB-1 (3-primary allylic + 2-secondary allylic + 9 primary alkylic). The reactivity of linear alkenes, with relatively longer alkyl chains [55] in the low temperature regime is mainly controlled by the classical alkane-like low temperature kinetics.

The primary alkylic H-atom abstractions from DIB-1 and DIB-2 result in the formation of $iC_8D_4$-1R, $iC_8D_3$-1R, respectively. These DIB radicals can either undergo β-scission reactions or react with $O_2$ to form alkenyl peroxy radicals. The alkenyl peroxy radicals of DIB cannot undergo a concerted $H\dot{O}_2$ elimination reaction via the formation of a five membered ring transition state, due to the absence of H-atoms. In the case of DIB-1, 60% of $iC_8D_4$-1R undergoes β-scission to form isobutene and 2-methyl-allyl radicals and ~16% to form a $C_7$ diene and methyl radical (see Fig. 5). The relatively lower flux of $iC_8D_4$-1R (24%) reacts with $O_2$ to form $iC_8D_4$-$1O_2$R, whereas, in the case of DIB-2, ~80% of $iC_8D_3$-1R reacts with $O_2$ to form $iC_8D_3$-$1O_2$R. $iC_8D_3$-$1O_2$R contributes to the low-temperature reactivity of DIB-2 through an H-atom shift via a six membered TS ring formation and cyclo-addition pathways. The β-scission reactions of DIB-1 radicals ($iC_8D_4$-1R) inhibit reactivity, as they compete with $O_2$ and $H\dot{O}_2$ addition pathways which contribute to greater reactivity at low temperatures, and hence, DIB-1 exhibit lower reactivity compared to DIB-2 in the low temperature regime (650 – 900 K).

### 4.4. Speciation data

To better understand the low temperature kinetics, the sampling experiments in ULille RCM for neat DIB-1 and DIB-2 were performed to identify and quantify the stable intermediate species formed during the ignition delay period, at $T_C = 700$ K, $p_C = 25$ bar, and $\varphi = 1.0$. All samples from the reacting mixture were extracted from the reaction chamber into a previously vacuumed heated sampling canister between 0.88 – 0.92 of the normalized IDT. The most abundant stable intermediates with a mole fraction higher than 50 ppm were used to validate the current model. Most of the experimentally observed intermediates correspond well with the DIB-1 model simulations, Fig. 10. The decomposition reactions of DIB-1 result in large quantities of isobutene ($iC_4H_8$) [18] and are slightly over-predicted (~30%) by the current model compared to the experiments that have estimated uncertainties of ± 15%. $\dot{O}H$ radical addition to the terminal vinylic site of DIB-1 and subsequent Waddington mechanism results in the production of 4,4-dimethyl-2-pentanone ($neC_7Y_4$) and

formaldehyde (HCHO). HCHO was observed in the MS chromatograms but was not quantified. neC$_7$Y$_4$, one of the Waddington products, is also well predicted (within ~20%).

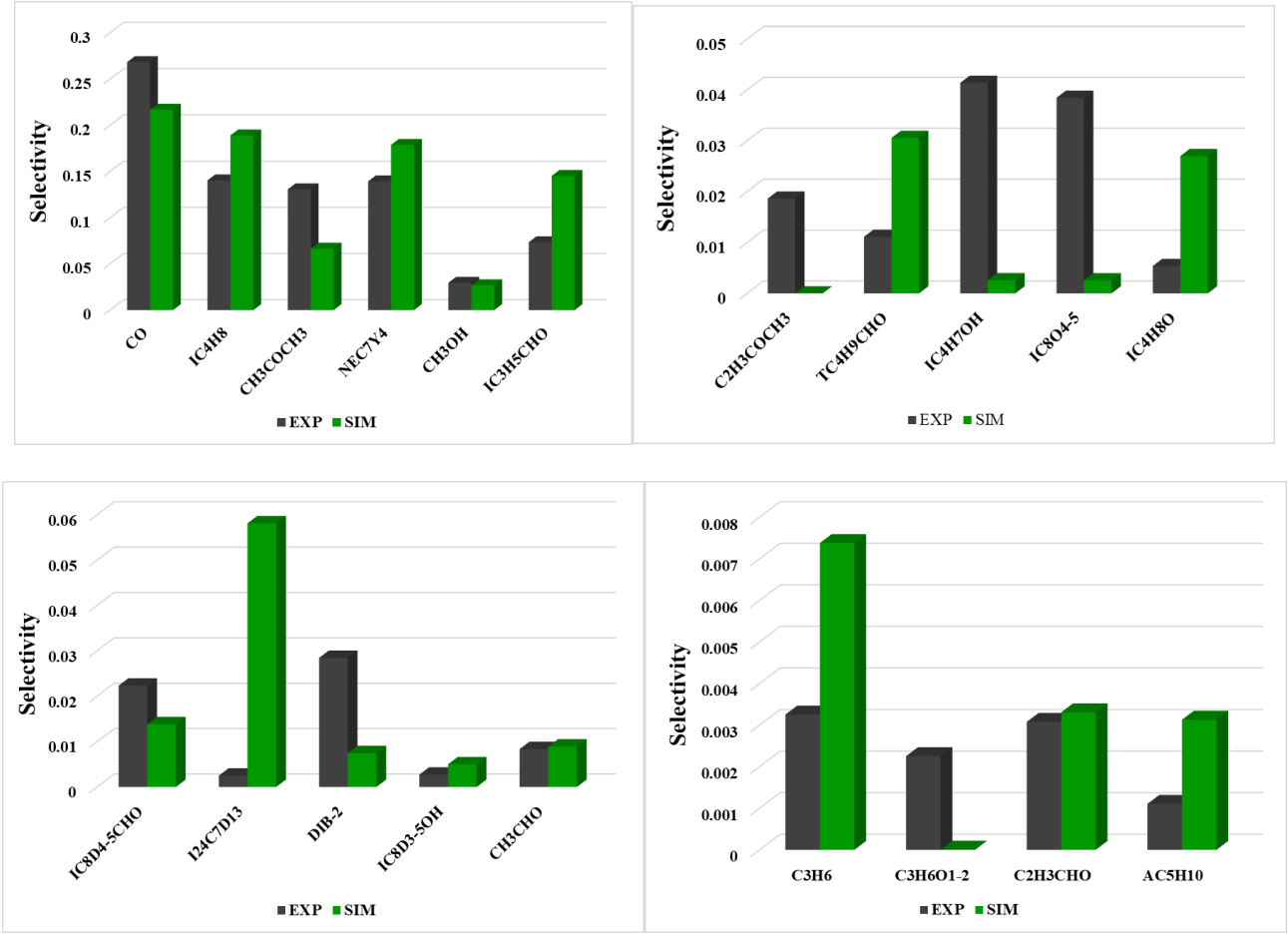


**Figure 10**: RCM species selectivity for DIB-1 at $T$c = 700 K, $p_C$ = 25 bar, $\varphi$ = 1.0 in air.

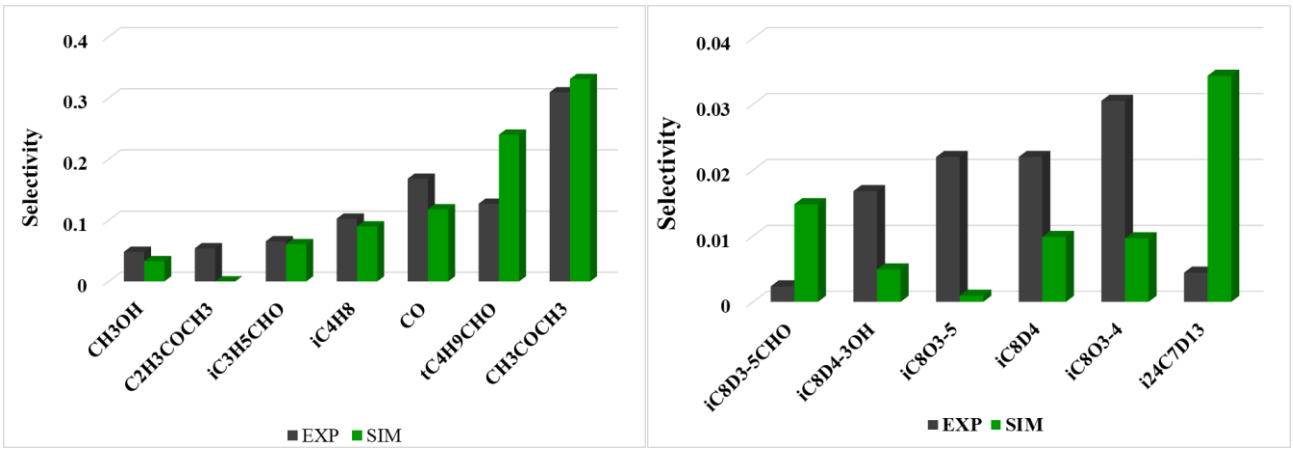

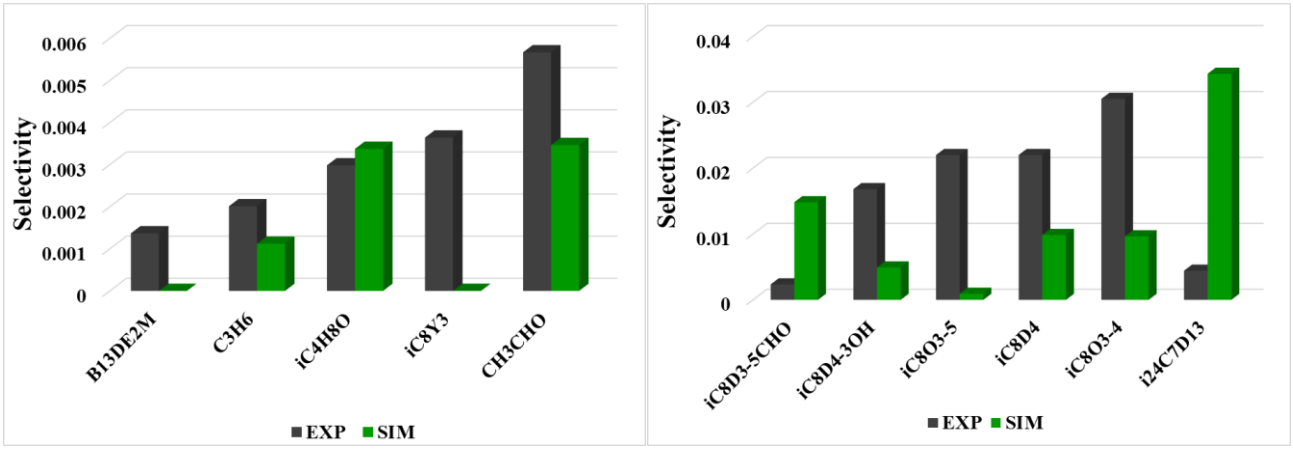


**Figure 11**: RCM species selectivity for DIB-2 at $Tc = 700$ K, $p_C = 25$ bar, $\varphi = 1.0$ in air.

In the case of DIB-2, at 700 K, conversion primarily proceeds via the Waddington mechanism and results in the production of $tC_4H_9CHO$ and acetone, which the current model well captures. In addition, other stable species in the model, such as $CH_3OH$, $C_3H_6$, $CH_3CHO$, $iC_4H_8$, a-$C_5H_{10}$, methyl-acrolein, etc., are well reproduced. However, the current model consistently under-predicts the oxirans and oxetans produced during DIB oxidation, for instance, 2-methyl-2-neopentyl-oxirane ($iC_8O4$-5) and 2-tertbutyl-3,3-dimethyl oxirane ($iC_8O3$-4). The current model predictions of oxiranes could be further improved by performing high-level theoretical calculations on the reaction rate constants for fuel addition reactions with $H\dot{O}_2$.

Figures 12 and 13 represent the validation of the DIB model developed in this study against the stable species profiles studied in the ICARE Orléans JSR setup at 10 atm, and temperature range 720 – 1200 K, at $\varphi = 0.5 – 2.0$; the fuel initial mole fraction was 1000 ppm for all experiments. The model is in good agreement with most of the species over a wide range of experimental conditions as shown in Figs. 12 and 13 ($\varphi$ = 1.0 and 10 atm), additional validation plots ($\varphi$ = 0.5 and 2.0 at 10 atm) of DIB-1 and the mixture (DIB-1 and DIB-2) are included in the Supplementary material.

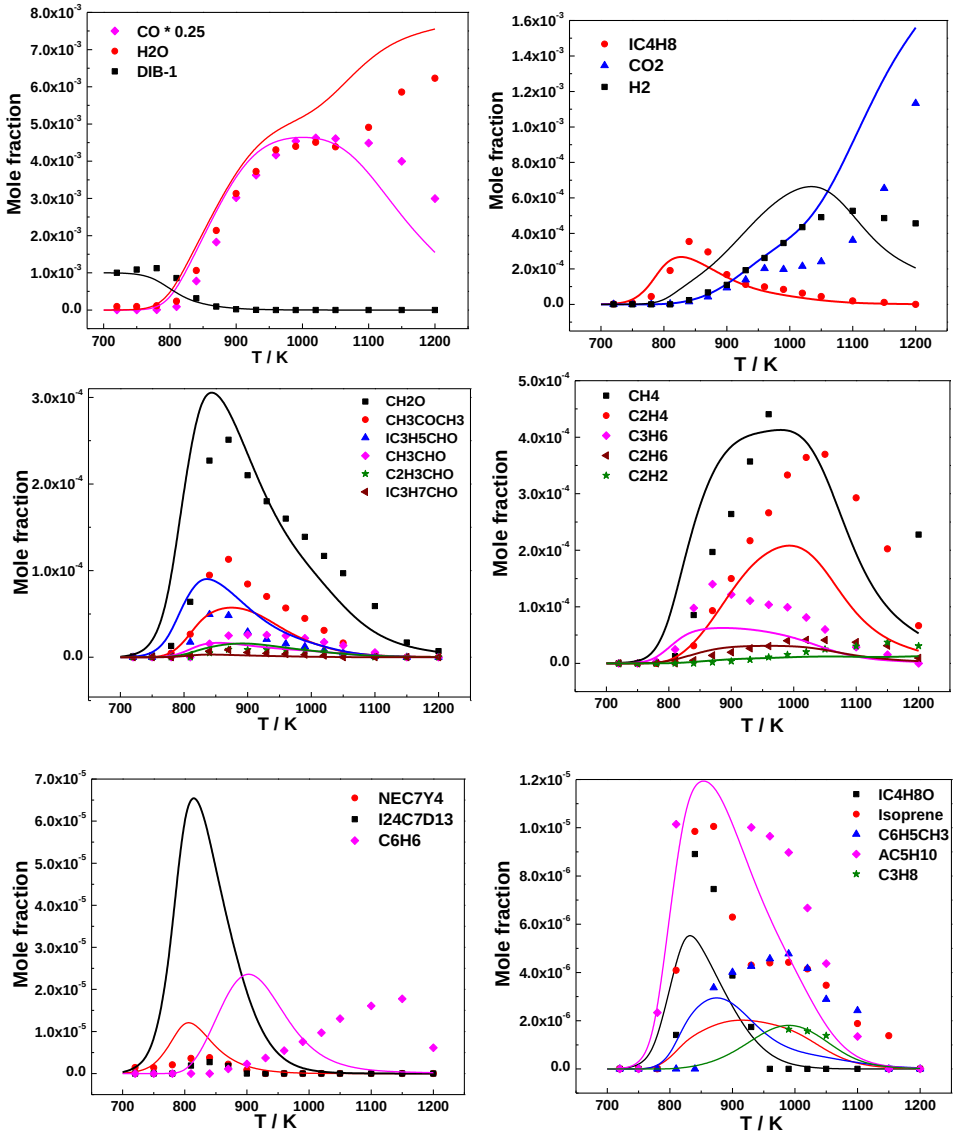


**Figure 12**: Neat DIB-1 oxidation species profiles for 1000 ppm DIB-1 and $\varphi$ = 1.0, at $p$ = 10 atm and $\tau$ = 0.7 s. Points are new experimental results, and lines represent current DIB model simulations.

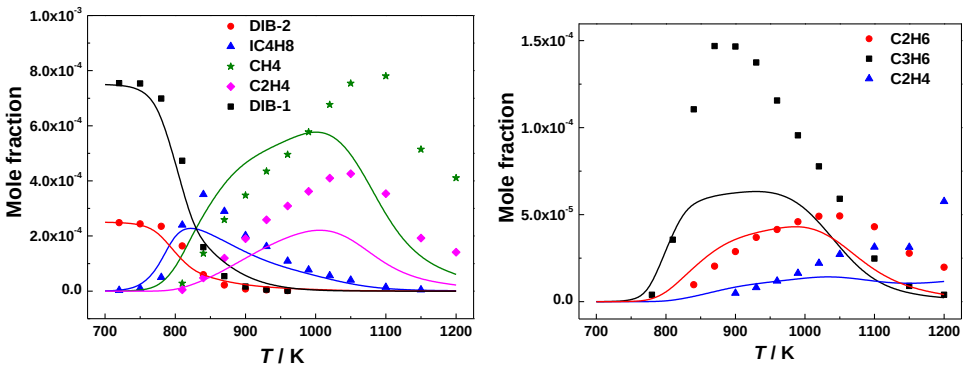

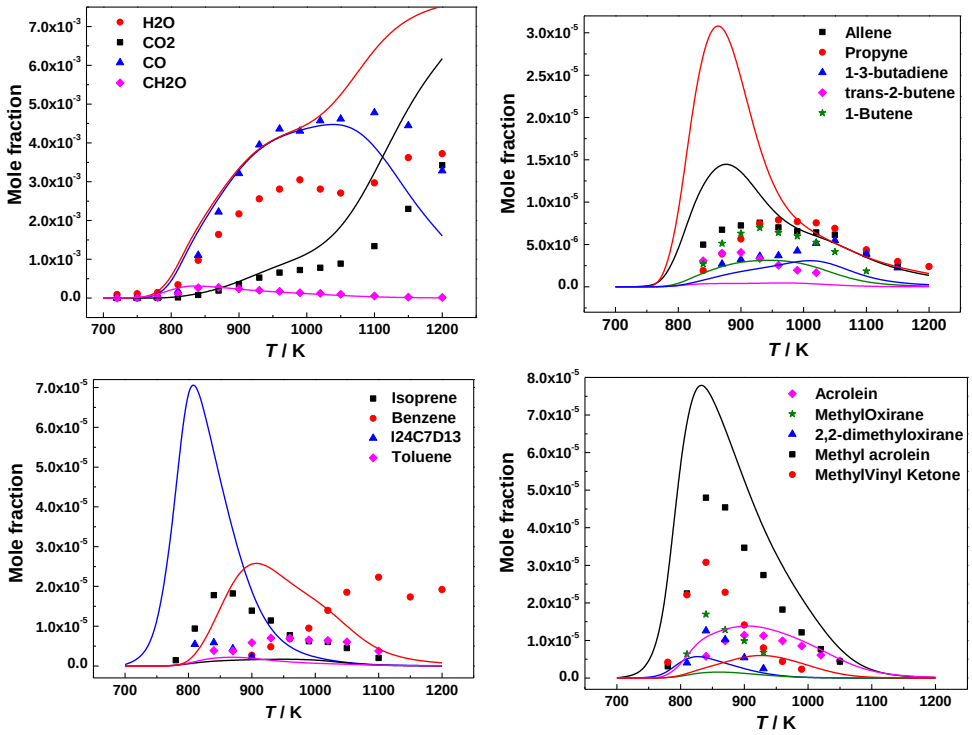


**Figure 13**: Oxidation species profiles for DIB mixture containing 750 ppm DIB-1 + 250 ppm DIB-2 at $\varphi$ = 1.0 in air 10 atm, $\tau$ = 0.7 s. Points are new experimental results, and lines represent current DIB model simulations.

The fuel conversion is dependent on the equivalence ratio. Conversion of neat DIB-1 and DIB mixture starts at ≈ 800 K and ≈ 780 K, respectively, for all equivalence ratios. A higher reactivity is observed as the mixtures get leaner at a given temperature, Fig. 12(a), Fig. 13(a), Fig. S1(a), Fig. S2(a) and Fig. S3(a). The fuel mole fraction profiles are well predicted by the model, indicating that the fuel consumption rate and its total reactivity are adequately considered during the development of the mechanism. The experimental speciation data provide further insight into the low temperature oxidation chemistry of DIB isomers. Yet, the current model could be further improved by performing high-level theoretical calculations to generate accurate thermochemical data and/or reaction rate coefficients for specific critical H-atom abstraction reactions. For instance, the H-atom abstraction reactions of the DIB isomers by $CH_3\dot{O}_2$ are highly sensitive, as discussed in the previous sections. We suggest future work to be directed to study this kind of reactivity, as it would be necessary for the development of kinetic mechanisms of large branched unsaturated hydrocarbons, such as DIB.

Other major intermediates directly formed from the fuel decomposition, such as $iC_4H_8$, $neC_7Y_4$, HCHO, $CH_3COCH_3$, acrolein, etc., are reproduced reasonably well (within a factor of two) compared to the experiments which have estimated uncertainties of ±15% for both neat DIB-1 and DIB isomer mixture experimental data, Figs. 12 and 13.

## 5. Conclusions

DIB is one of the six fuel blendstocks short-listed for Co-Optima research. DIB isomers are also important intermediates in the oxidation of iso-octane; however, typical low-temperature kinetics is limited in the literature DIB sub-mechanisms. Major discrepancies were noted in the IDT predictions of various literature surrogate models when validated against the new DIB-1 data from this study. This study presents a wide range of low temperature and high-pressure experimental measurements, which can be a direct validation target for the multicomponent surrogate models featuring DIB-1 and/or DIB-2. A kinetic model has been developed which can accurately reproduce the observed autoignition behavior and species mole-fraction profiles.

DIB-2 shows higher reactivity in comparison to DIB-1 for the conditions inspected in this study. The influence of the position of the double bond for DIB was analysed via kinetic analyses performed at 800 K shows that the (i) fate of the DIB alkyl radical (β-scission or reaction with $O_2$) and (ii) abstraction reactions (followed by reactions with hydroperoxyl radicals) are the major reaction channels that determine reactivity at these conditions. The current model can well capture the global reactivity targets of DIB isomers such as IDTs from two independent RCM facilities and local reactivity targets such as speciation from an RCM and a JSR at various conditions. Our model is in good agreement with the most stable intermediates formed in the RCM sampling experiments and JSR experiments performed for the DIB isomers. However, the model needs further investigation to improve the various radical addition pathways to the double-bond, and H-atom abstraction reactions highlighted previously. These reaction classes are suitable candidates for future work.

## Acknowledgments

The authors at NUI Galway recognize funding support from Science Foundation Ireland (SFI) via project numbers 15/IA/3177 and 16/SP/3829. The work at LLNL was performed under the auspices of the U.S. Department of Energy (DOE) by Lawrence Livermore National Laboratory under Contract DE-AC52-07NA27344 and was conducted as part of the Co-Optimization of Fuels & Engines (Co-Optima) initiative sponsored by the DOE Office of Energy Efficiency and Renewable Energy (EERE), Bioenergy Technologies and Vehicle Technologies Offices. This research performed in ULille was funded by TOTAL Marketing Services and is a contribution to the CPER research project Climibio. HS and GV thank the Région Hauts-de-France, and the Ministère de l'Enseignement Supérieur et de la Recherche (CPER Climibio), and the European Fund for Regional Economic Development for their financial support. The study was supported by the grant from the Russian Science Foundation (project No. 19-79-00325). The authors would also like to acknowledge the financial support from the Energy Agency via the Centre for Combustion Science and Technology [Project KC-CECOST 22538-4], Sweden. M.S., A.B, and P.H acknowledge funding by the Swiss Federal Office of Energy (SI/501269-01). The pyrolysis measurements (presented in Part II) were carried out at the VUV (x04db) beamline of the Swiss Light Source storage ring, located at Paul Scherrer Institute in Villigen (Switzerland).

## Declaration of Competing Interest

The authors declare that they have no known competing financial interests or personal relationships that could have appeared to influence the work reported in this paper.

## Disclaimer

This report was prepared as an account of work sponsored by an agency of the United States Government. Neither the United States Government nor any agency thereof, nor any of their employees, makes any warranty, express or implied, or assumes any legal liability or responsibility for the accuracy, completeness, or usefulness of any information, apparatus, product, or process disclosed or represents that its use would not infringe privately owned rights. Reference herein to any specific commercial product, process, or service by trade name, trademark, manufacturer, or otherwise does not necessarily constitute or imply its endorsement, recommendation, or favoring by

the United States Government or any agency thereof. The views and opinions of authors expressed herein do not necessarily state or reflect those of the United States Government or any agency thereof.

## References


[1] W.K. Metcalfe, W.J. Pitz, H.J. Curran, J.M. Simmie, C.K. Westbrook, The development of a detailed chemical kinetic mechanism for diisobutylene and comparison to shock tube ignition times, Proceedings of the Combustion Institute, 31 (2007), 377-384.
[2] J. Farrell, J. Holladay, R. Wagner, Fuel blendstocks with the potential to optimize future gasoline engine performance: identification of five chemical families for detailed evaluation, US Department of Energy, Washington, DC, doi:https://doi.org/10.2172/1434413(2018).
[3] D.J. Gaspar, B.H. West, D. Ruddy, T.J. Wilke, E. Polikarpov, T.L. Alleman, A. George, E. Monroe, R.W. Davis, D. Vardon, Top Ten Blendstocks Derived From Biomass For Turbocharged Spark Ignition Engines: Bio-blendstocks With Potential for Highest Engine Efficiency, Pacific Northwest National Lab.(PNNL), Richland, WA (United States), doi:https://doi.org/10.2172/1567705(2019).
[4] J. Farrell, R. Wagner, C. Moen, D. Gaspar, A Transportation Future with Science in the Driver's Seat: Mapping a Viable Route Forward for Affordable, Efficient, and Clean Fuels and Engines, DOE/EERE-2046, (2020).
[5] J.C.G. Andrae, R.A. Head, HCCI experiments with gasoline surrogate fuels modeled by a semidetailed chemical kinetic model, Combustion and Flame, 156 (2009), 842-851.
[6] L.R. Cancino, M. Fikri, A.A.M. Oliveira, C. Schulz, Ignition delay times of ethanol-containing multi-component gasoline surrogates: Shock-tube experiments and detailed modeling, Fuel, 90 (2011), 1238-1244.
[7] M. Fikri, J. Herzler, R. Starke, C. Schulz, P. Roth, G.T. Kalghatgi, Autoignition of gasoline surrogates mixtures at intermediate temperatures and high pressures, Combustion and Flame, 152 (2008), 276-281.
[8] E. Hu, G. Yin, Z. Gao, Y. Liu, J. Ku, Z. Huang, Experimental and kinetic modeling study on 2,4,4-trimethyl-1-pentene ignition behind reflected shock waves, Fuel, 195 (2017), 97-104.
[9] H. Li, Y. Qiu, Z. Wu, S. Wang, X. Lu, Z. Huang, Ignition delay of diisobutylene-containing multicomponent gasoline surrogates: Shock tube measurements and modeling study, Fuel, 235 (2019), 1387-1399.
[10] B.-J. Zhong, D. Zheng, A chemical mechanism for ignition and oxidation of multi-component gasoline surrogate fuels, Fuel, 128 (2014), 458-466.
[11] J.C.G. Andrae, Development of a detailed kinetic model for gasoline surrogate fuels, Fuel, 87 (2008), 2013-2022.
[12] J.C.G. Andrae, T. Kovács, Evaluation of Adding an Olefin to Mixtures of Primary Reference Fuels and Toluene To Model the Oxidation of a Fully Blended Gasoline, Energy & Fuels, 30 (2016), 7721-7730.
[13] S. Ren, S.L. Kokjohn, Z. Wang, H. Liu, B. Wang, J. Wang, A multi-component wide distillation fuel (covering gasoline, jet fuel and diesel fuel) mechanism for combustion and PAH prediction, Fuel, 208 (2017), 447-468.
[14] M. Mehl, W.J. Pitz, C.K. Westbrook, K. Yasunaga, C. Conroy, H.J. Curran, Autoignition behavior of unsaturated hydrocarbons in the low and high temperature regions, Proc. Combust. Inst., 33 (2011), 201-208.
[15] G. Mittal, C.-J. Sung, Homogeneous charge compression ignition of binary fuel blends, Combustion and Flame, 155 (2008), 431-439.
[16] Y. Wu, M. Yang, X. Yao, Y. Liu, C. Tang, Comparative studies on the ignition characteristics of diisobutylene isomers and iso-octane by using a rapid compression machine, Fuel, 276 (2020), 118008.
[17] H. Song, R. Dauphin, G. Vanhove, A kinetic investigation on the synergistic low-temperature reactivity, antagonistic RON blending of high-octane fuels: Diisobutylene and cyclopentane, Combustion and Flame, 220 (2020), 23-33.

[18] N. Lokachari, S. Panigrahy, G. Kukkadapu, G. Kim, S.S. Vasu, W.J. Pitz, H.J. Curran, The influence of iso-butene kinetics on the reactivity of di-isobutylene and iso-octane, Combustion and Flame, 222 (2020), 186-195.
[19] N. Lokachari, G. Kukkadapu, H. Song, G. Vanhove, G. Dayma , Z. Serinyel, K. Zhang, R. Dauphin, B. Etz, S. Kim, M. Steglich, A. Bodi, G. Fioroni, P. Hemberger, S.S. Matveev, A.A. Konnov, P. Dagaut, W.J. Pitz, H.J. Curran, A comprehensive experimental and kinetic modeling study of di-isobutylene isomers: Part 2, Work in progress, (2021).
[20] C. Morley, Gaseq, Available at http://www.gaseq.co.uk/, (2004).
[21] Y. Fenard, M.A. Boumehdi, G. Vanhove, Experimental and kinetic modeling study of 2-methyltetrahydrofuran oxidation under engine-relevant conditions, Combustion and Flame, 178 (2017), 168-181.
[22] Y. Fenard, H. Song, H. Minwegen, P. Parab, C. Sampaio Mergulhão, G. Vanhove, K.-A. Heufer, 2,5-Dimethyltetrahydrofuran combustion: Ignition delay times at high and low temperatures, speciation measurements and detailed kinetic modeling, Combustion and Flame, 203 (2019), 341-351.
[23] C.S. Mergulhão, H.-H. Carstensen, H. Song, S.W. Wagnon, W.J. Pitz, G. Vanhove, Probing the antiknock effect of anisole through an ignition, speciation and modeling study of its blends with isooctane, Proceedings of the combustion institute, 38(1) (2021), 739-748.
[24] D. Lee, S. Hochgreb, Rapid Compression Machines: Heat Transfer and Suppression of Corner Vortex, Combustion and Flame, 114 (1998), 531-545.
[25] N. Bourgeois, S.S. Goldsborough, H. Jeanmart, F. Contino, CFD simulations of Rapid Compression Machines using detailed chemistry: Evaluation of the 'crevice containment' concept, Combustion and Flame, 189 (2018), 225-239.
[26] S.S. Goldsborough, S. Hochgreb, G. Vanhove, M.S. Wooldridge, H.J. Curran, C.-J. Sung, Advances in rapid compression machine studies of low- and intermediate-temperature autoignition phenomena, Progress in Energy and Combustion Science, 63 (2017), 1-78.
[27] G. Vanhove, M. Ribaucour, R. Minetti, On the influence of the position of the double bond on the low-temperature chemistry of hexenes, Proceedings of the Combustion Institute, 30 (2005), 1065-1072.
[28] J.T. Scanlon, D.E. Willis, Calculation of Flame Ionization Detector Relative Response Factors Using the Effective Carbon Number Concept, Journal of Chromatographic Science, 23 (1985), 333-340.
[29] P. Dagaut, M. Cathonnet, J.P. Rouan, R. Foulatier, A. Quilgars, J.C. Boettner, F. Gaillard, H. James, A jet-stirred reactor for kinetic studies of homogeneous gas-phase reactions at pressures up to ten atmospheres (≈1 MPa), Journal of Physics E: Scientific Instruments, 19 (1986), 207-209.
[30] J. Bugler, B. Marks, O. Mathieu, R. Archuleta, A. Camou, C. Grégoire, K.A. Heufer, E.L. Petersen, H.J. Curran, An ignition delay time and chemical kinetic modeling study of the pentane isomers, Combustion and Flame, 163 (2016), 138-156.
[31] K. Zhang, C. Banyon, U. Burke, G. Kukkadapu, S.W. Wagnon, M. Mehl, H.J. Curran, C.K. Westbrook, W.J. Pitz, An experimental and kinetic modeling study of the oxidation of hexane isomers: Developing consistent reaction rate rules for alkanes, Combustion and Flame, 206 (2019), 123-137.
[32] R. Fang, G. Kukkadapu, M. Wang, S.W. Wagnon, K. Zhang, M. Mehl, C.K. Westbrook, W.J. Pitz, C.-J. Sung, Fuel molecular structure effect on autoignition of highly branched iso-alkanes at low-to-intermediate temperatures: Iso-octane versus iso-dodecane, Combustion and Flame, 214 (2020), 152-166.
[33] E.R. Ritter, THERM: a computer code for estimating thermodynamic properties for species important to combustion and reaction modeling, Journal of chemical information and computer sciences, 31 (1991), 400-408.

[34] Y. Li, H.J. Curran, Extensive Theoretical Study of the Thermochemical Properties of Unsaturated Hydrocarbons and Allylic and Super-Allylic Radicals: The Development and Optimization of Group Additivity Values, J. Phys. Chem. A, 122 (2018), 4736-4749.
[35] S.M. Burke, J.M. Simmie, H.J. Curran, Critical Evaluation of Thermochemical Properties of C1–C4 Species: Updated Group-Contributions to Estimate Thermochemical Properties, Journal of Physical and Chemical Reference Data, 44 (2015), 013101.
[36] C. Cavallotti, F. Leonori, N. Balucani, V. Nevrly, A. Bergeat, S. Falcinelli, G. Vanuzzo, P. Casavecchia, Relevance of the Channel Leading to Formaldehyde + Triplet Ethylidene in the O(3P) + Propene Reaction under Combustion Conditions, The Journal of Physical Chemistry Letters, 5 (2014), 4213-4218.
[37] J. Zádor, S.J. Klippenstein, J.A. Miller, Pressure-Dependent OH Yields in Alkene + $HO_2$ Reactions: A Theoretical Study, The Journal of Physical Chemistry A, 115 (2011), 10218-10225.
[38] J. Badra, F. Khaled, B.R. Giri, A. Farooq, A shock tube study of the branching ratios of propene + OH reaction, Physical Chemistry Chemical Physics, 17 (2015), 2421-2431.
[39] S.S. Vasu, L.K. Huynh, D.F. Davidson, R.K. Hanson, D.M. Golden, Reactions of OH with Butene Isomers: Measurements of the Overall Rates and a Theoretical Study, The Journal of Physical Chemistry A, 115 (2011), 2549-2556.
[40] C.-W. Zhou, J.M. Simmie, K.P. Somers, C.F. Goldsmith, H.J. Curran, Chemical Kinetics of Hydrogen Atom Abstraction from Allylic Sites by $^3O_2$; Implications for Combustion Modeling and Simulation, The Journal of Physical Chemistry A, 121 (2017), 1890-1899.
[41] J. Badra, A. Farooq, Site-specific reaction rate constant measurements for various secondary and tertiary H-abstraction by OH radicals, Combustion and Flame, 162 (2015), 2034-2044.
[42] R. Sivaramakrishnan, J.V. Michael, Rate Constants for OH with Selected Large Alkanes: Shock-Tube Measurements and an Improved Group Scheme, The Journal of Physical Chemistry A, 113 (2009), 5047-5060.
[43] K. Wang, S.M. Villano, A.M. Dean, The Impact of Resonance Stabilization on the Intramolecular Hydrogen-Atom Shift Reactions of Hydrocarbon Radicals, ChemPhysChem, 16 (2015), 2635-2645.
[44] Y. Li, C.-W. Zhou, K.P. Somers, K. Zhang, H.J. Curran, The oxidation of 2-butene: A high pressure ignition delay, kinetic modeling study and reactivity comparison with isobutene and 1-butene, Proceedings of the Combustion Institute, 36 (2017), 403-411.
[45] D. Schleier, P. Constantinidis, N. Faßheber, I. Fischer, G. Friedrichs, P. Hemberger, E. Reusch, B. Sztáray, K. Voronova, Kinetics of the a-$C_3H_5$ + $O_2$ reaction, investigated by photoionization using synchrotron radiation, Physical Chemistry Chemical Physics, 20 (2018), 10721-10731.
[46] D. Schleier, E. Reusch, M. Gerlach, T. Preitschopf, D.P. Mukhopadhyay, N. Faßheber, G. Friedrichs, P. Hemberger, I. Fischer, Kinetics of 1- and 2-methylallyl + $O_2$ reaction, investigated by photoionisation using synchrotron radiation, Physical Chemistry Chemical Physics, 23 (2021), 1539-1549.
[47] C.-J. Chen, J.W. Bozzelli, Thermochemical Property, Pathway and Kinetic Analysis on the Reactions of Allylic Isobutenyl Radical with $O_2$: an Elementary Reaction Mechanism for Isobutene Oxidation, The Journal of Physical Chemistry A, 104 (2000), 9715-9732.
[48] K. Zhang, C. Banyon, J. Bugler, H.J. Curran, A. Rodriguez, O. Herbinet, F. Battin-Leclerc, C. B'Chir, K.A. Heufer, An updated experimental and kinetic modeling study of n-heptane oxidation, Combustion and Flame, 172 (2016), 116-135.
[49] X. Sun, W. Zong, J. Wang, Z. Li, X. Li, Pressure-dependent rate rules for cycloaddition, intramolecular H-shift, and concerted elimination reactions of alkenyl peroxy radicals at low temperature, Physical Chemistry Chemical Physics, 21 (2019), 10693-10705.
[50] C.F. Goldsmith, W.H. Green, S.J. Klippenstein, Role of $O_2$ + QOOH in Low-Temperature Ignition of Propane. 1. Temperature and Pressure Dependent Rate Coefficients, The Journal of Physical Chemistry A, 116 (2012), 3325-3346.

[51] C.-W. Zhou, Y. Li, E. O'Connor, K.P. Somers, S. Thion, C. Keesee, O. Mathieu, E.L. Petersen, T.A. DeVerter, M.A. Oehlschlaeger, G. Kukkadapu, C.-J. Sung, M. Alrefae, F. Khaled, A. Farooq, P. Dirrenberger, P.-A. Glaude, F. Battin-Leclerc, J. Santner, Y. Ju, T. Held, F.M. Haas, F.L. Dryer, H.J. Curran, A comprehensive experimental and modeling study of isobutene oxidation, Combustion and Flame, 167 (2016), 353-379.
[52] J. Zádor, A.W. Jasper, J.A. Miller, The reaction between propene and hydroxyl, Physical Chemistry Chemical Physics, 11 (2009), 11040-11053.
[53] H. Sun, J.W. Bozzelli, C.K. Law, Thermochemical and Kinetic Analysis on the Reactions of O2 with Products from OH Addition to Isobutene, 2-Hydroxy-1,1-dimethylethyl, and 2-Hydroxy-2-methylpropyl Radicals: $HO_2$ Formation from Oxidation of Neopentane, Part II, The Journal of Physical Chemistry A, 111 (2007), 4974-4986.
[54] K. Wang, S.M. Villano, A.M. Dean, Experimental and kinetic modeling study of butene isomer pyrolysis: Part II. Isobutene, Combustion and Flame, 176 (2017), 23-37.
[55] S. Dong, K. Zhang, P.K. Senecal, G. Kukkadapu, S.W. Wagnon, S. Barrett, N. Lokachari, S. Panigaphy, W.J. Pitz, H.J. Curran, A comparative reactivity study of 1-alkene fuels from ethylene to 1-heptene, Proceedings of the Combustion Institute, 38 (2021), 611-619.